Published in AJSE, Vol:23, Issue: 2
Received on 11th July 2023
Revised on 26th August 2024
Published on 30th August 2024

AIUB JOURNAL OF SCIENCE AND ENGINEERING
ISSN: 1608 – 3679 (print) 2520 – 4890 (Online)

Datalogger prototyping for NH_3 ground-level concentrations measurements and comparison with NH_3-IASI generated datamaps

Imene Nadjah MENAKH [1], Noureddine BENABADJI [1], Farid RAHAL [1]

[1] Laboratory of Analysis and Application of Radiations, University of Sciences and Technology of Oran, Mohamed Boudiaf, Oran, Algeria

***Abstract*— Ammonia (NH_3) is a highly dangerous gas due to its toxicity and irritating properties which cause severe eye burns and respiratory problems (throat and lung damages) when inhaled in high concentrations. It is a colorless gas, with a strong suffocating odor. It is also a flammable gas (potentially forming explosive mixtures with air when heated). Ammonia readily dissolves in water to form ammonium hydroxide solution (NH_4OH), a highly corrosive agent that can damage metallic structures such as bridges, boats, water tanks, etc… It can also react with other atmospheric pollutants, primarily SO_2 and NOx, generating fine particulate matter which can pass through the lungs into the bloodstream, posing great health risks. On the other hand, it is also considered as an industrial useful hydrogen carrier of energy, and an additive for coal-fired power plants, and is slowly repurposed from its natural role as a fertilizer in the agricultural industry to a "green and clean" fuel source. In this article, we describe in detail the use of an electrochemical sensor driven by a microcontroller. The principle of the measurement system is a chemical oxidation of catalyst metals, where conductivity varies with the target gas concentration. Mathematical calculations are also provided to convert the 10-bit numerical counts to meaningful NH_3 concentrations in ppm, taking into account the temperature dependency correction. As a final stage, 4 months of data acquisition has been carried out in the petrochemical industrial city of Arzew.**

***Index Terms*— Air pollution, Ammonia, Electrochemical sensor, Datalogger, Temperature correction**

I. Introduction

As both anthropogenic pollution, such as vehicle emissions, coal combustion, industrial chemical processes, etc… [1]-[6]) and natural sources of air pollution continue to rise, like forest fires, volcanic activity, decay of organic matter, etc… [7] [8]), there has been a growing interest in various types of gas sensors. Over the past century, numerous sensors dedicated to detecting gas pollutants have been developed [9] [10] with continuous advancements and optimizations in their processing technologies. Traditional devices, such as those using spectroscopy and chromatography, have been employed to detect various pollutant gases, but they suffer from complicated preparation techniques and rely on bulky expensive equipment. Today, a variety of modern gas sensors are available: Metal oxide-based sensors (MOX), optical, electrochemical, etc…, where MOX type is still the most widely used, due to its implementation simplicity, compact size, low-cost, long lifespan, etc… Thus, an increasing number of portable gas monitors are being introduced to the global market, now featuring data logging capabilities and dedicated software that enable users to analyze data more effectively and with greater ease.

In this article, we focus on ammonia (NH_3) sensing using a low-cost MOX-type detector. The MQ series (MQ-135, MQ-136, MQ-137, …) are among the most widely used sensors for NH_3 detection due to their affordability. The TGS series (TGS-826, TGS-2444, TGS2602, etc…) is also valued for its higher selectivity, but tend to be more expensive. Industrial plants employ the most accurate and sensitive NH_3 sensors, often configured in a mesh network topology to ensure broader and more comprehensive monitoring coverage. A wide range of sensitive materials, such as SnO_2, ZnO, WO_3, TiO_2, and MoO_3, are commonly used in the fabrication process [11] [12].

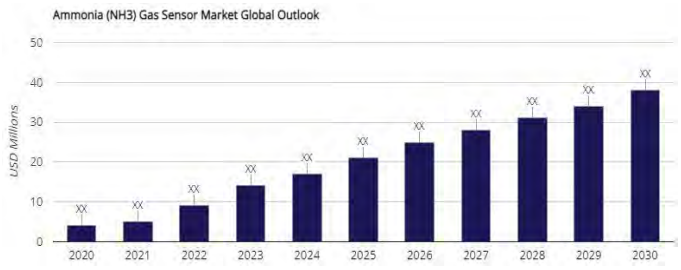

Fig.1: The ammonia gas sensors market trends with a forecast period upto 2030. [13]

Manuscript received : July 11th, 2023
Manuscript revision1 : August 08th, 2024
Manuscript revision2 : August 25th, 2024
Manuscript accepted : August 26th, 2024
Imene Nadjah MENAKH, PhD student, holds a Master Degree in the field of Physics (email: imanenadjah.menakh@univ-usto.dz)
Pr. Noureddine BENABADJI, Laboratory of Analysis and Application of Radiations (email: noureddine.benabadji@univ-usto.dz)
Dr. Farid RAHAL, Laboratory of Analysis and Application of Radiations (email: farid.rahal@univ-usto.dz).

II. MATERIAL AND METHOD

II.1- The hardware design:

The prototype of this versatile datalogger comprises several key components, as shown in figure2: **(a)** the microcontroller (with its minimal essential system components), **(b)** the ammonia sensor (with integrated signal conditioning), **(c)** the temperature/humidity combo sensors (for correcting ammonia concentration measurements), **(d)** the real time clock (for precise timestamping of measurements) with the non-volatile memory (for data storage) and **(e)** the serial interface for connecting to Windows, Mac, Linux, or Android devices (either via a wired USB/TTL connection or wirelessly through Bluetooth).

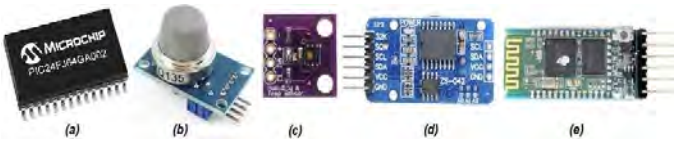

Fig.2: The key components to build a programmable datalogger.

The power supply is provided by an internal Li-Po battery, or by a 5V charger for long term data acquisitions.

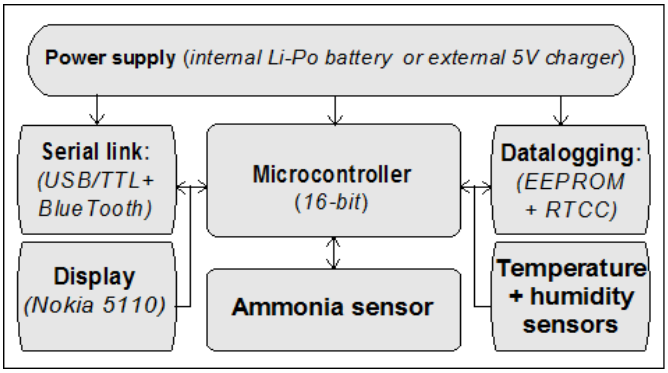

Fig.3: synoptic diagram of the prototype.

For the target gas monitoring, we have chosen the MQ-135 sensor [14] in order to measure the ammonia (NH_3) concentrations in ambient air. It is a small and low-cost electrochemical gas sensor (MOX type), which have a good sensitivity to NH_3 (10 to 1000 ppm). It uses tin dioxide (SnO2) as the sensing material, which reacts with NH_3 molecules in the ambient air. The sensor's conductivity increases when the gas concentration rises, thus the equivalent internal resistance (Rs) decreases. In order to accelerate the chemical reaction, an internal heater resistance (Rh) must be precisely controlled with a 5V heater voltage (Vh), to provide the suitable working temperature for NH_3 sensing. As the NH_3 concentrations measures are temperature and humidity dependent, so we have added a temperature/humidity combo sensor, based on a HDC1080 module [15], for the measurement's corrections.

We used a 16-bit microcontroller (PIC24FJ64GA002) [16], to drive all these parts. Its filter capacitor C9 should have a low ESR, and chosen as a multi-layer ceramic or a tantalum type capacitor. A key point to note about this microcontroller: its PPS feature (*Peripheral Pin Select*) which ease the PCB drawing. It also costs less than the last recently 8-bit microcontrollers put on the market, which also have this feature, but still are limited in flash ROM and RAM memories capacity. Programming in a high level language and using a graphic display require a certain amount of ROM and RAM.

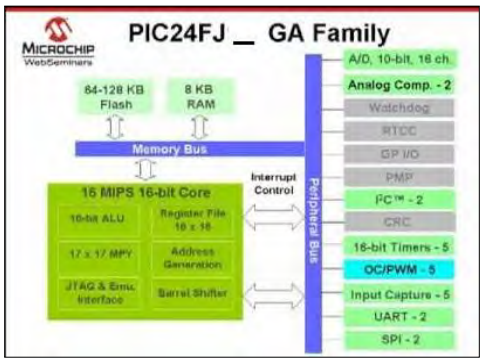

Fig.4: The architectural diagram of the PIC24FJ64GA002 [16]

In order to lower the power consumption, the PICmicro is configured with its highest system frequency, and uses the deep sleep mode between required periodic jobs. It is powered with a XC6206 micro-power low drop-out voltage regulator of 3.3V [17] characterized by a quiescent current of 1.6 µA. We need also an efficient step-up voltage regulator of 5V [18] to power the NH_3 sensor, through a P-mosfet switch (T1). This optional switch (chosen with a very low RdsON, and a VgsTH of at least 1.3V [19]) allows us to drive the NH_3 sensor with an experimental periodic Ton/Toff (instead of the standard continuous driving) and observe how the measures can be affected.

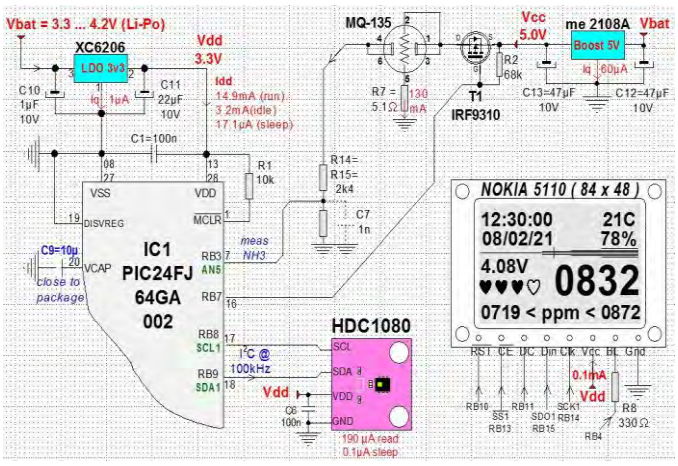

Fig.5: driving circuit for the MQ-135 sensor, and the temperature/humidity sensors.

The resistance R7 slightly reduces the heater current to 130 mA (instead of 150mA) but has been provided here in order to allow a simple protection to T1 in case of a short-circuit in the internal resistance heater Rh. Hence, an additional option may be added to control Rh simply by measuring its voltage Vh

(this precaution is mandatory for medical and industrial critical devices). The voltage divider R14/R15 keeps the voltage variation seen by the analog pin (AN5) always less than Vdd.

Among the main characteristics of any datalogger are the accuracy of the real time clock and calendar (RTCC) for long-term data acquisition time stamps, the non-volatile memory capacity for raw data storage, and the battery life if it is an embedded standalone device type:

a- The RTCC module is based on a DS3231 [20], which doesn't need an external 32768 Hz quartz, and is characterized with a high precision of 2 ppm, better than the popular DS1307 (20ppm, and requires an external 32768 Hz quartz). With 2ppm, we expect a clock drift of only 1 minute per year !

b- The external EEPROM is based on a 24C32 [21], which provides a memory capacity of 4kBytes. As we want to store the 10-bit numerical count of NH3 measures, the 7-bit data of temperature, the 7-bit data of relative humidity, and the 16-bit of time stamps, so we need 40 bits (or 5 bytes) for each packet to store. We chose a duration of 15 minutes for periodic storage (while measures are acquired in real time, each second, and can be displayed on a PC through a wired serial link or a wireless Bluetooth link). So we have 96 packets (or 480 bytes) stored per day, and a total of 768 packets (or 3840 bytes) stored in 8 days. If necessary, higher memory capacity EEPROM may be chosen for more data acquisition (a compatible pin to pin 24LC1025 has 128kBytes, useful to store up to 26214 packets, stored in 273 days), or external flash ROM with memory capacity of several Mbytes, but are more energy-consuming (it is worse if we choose a micro SD card, because it is generally less reliable in the long run).

c- Using a battery life calculator [22], or a power profiler kit [23], the proposed datalogger can be used up to 31 days with a LiPo battery of 4000mAh, when configuring the ratio Toff = 9s (where I = 145 mA for 0.34s in run mode, then 51µA in sleep mode) over a periodic data acquisition T = 10s.

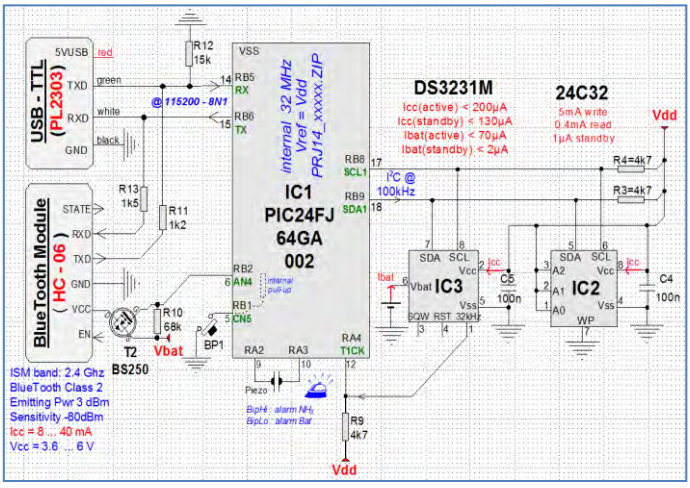

Fig.6: Other datalogging required modules and the serial link options to a PC.

II.2- The firmware implementation:

Regarding the total current consumption, attention must be carefully taken, not only to the choice of components and circuits involved, but also to the way in which the firmware is implemented [24]. Some articles [25] [26] show that, until a certain limit, the energy consumption decreases as the operating frequency increases. This is why we chose the max. operating frequency for the microcontroller (PLL @ 32MHz) at run times, then use deep sleep mode for idle times. The graphic display is a NOKIA 5110 monochrome LCD type, characterized with a very low current consumption (about 0.1mA when enabled, and 34 µA when disabled). There is no embedded keypad, as the initial configuration is set with a PC, through the serial link. Nevertheless, one pushbutton BP1 is provided to swap between multiple screens, using a relatively simple and intuitive solution. Rotary encoder has not been chosen as it needs at least three GPIO pins to be driven.

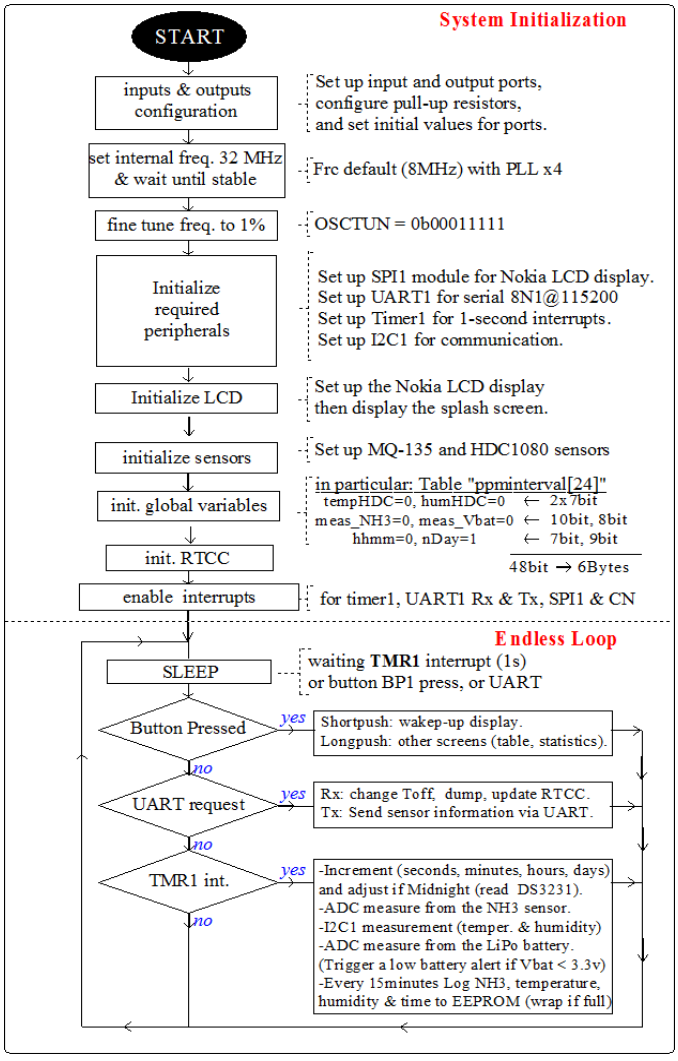

Fig.7: A simplified algorithm illustrating the operation of the datalogger.

Figure 8 shows an example of a main menu with a title and a list of four options. To move around each of these four options (in circular mode), short push (< 2s) is needed. If a long push (> 4s) is given, the option (marked with an asterisk)

is selected and bring up a secondary menu. The same procedure is also used here to bring up a third menu, etc… ; Timeout (about 8s) is sufficient to go back to the main menu, if the pushbutton is not pressed. (A double-clic could also be used for this task, but has not been developed).

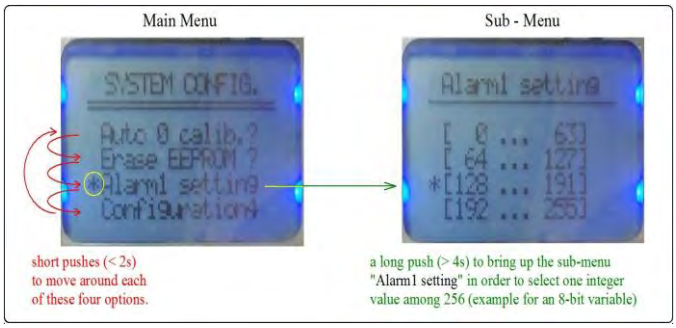

Fig.8: cycling (with short pushes) through the 4 options in the main menu, then selecting an option with a long push.

Figure 9 shows an example of how to choose an integer value (among 256) using the principle of dichotomy (to go fast). First, divide the full range [0 … 255] into four sub-ranges [0…63] [64…127] [128…191] [192…255] to fill the four options lines. After selecting one of these sub-ranges, you get a secondary menu with new four and smaller sub-ranges. For instance, if you have selected [0…63], then you obtain [0…15] [16…31] [32…47] [48…63] in this secondary menu. And so on … You finally need 4 successive menus to be able to choose a single 8-bit integer value. In order to generalize this concept, let denote by L the number of lines in a menu, and by M the number of successive menus, then the full range of integer numbers you can deal with is: [0, …, L^M -1].

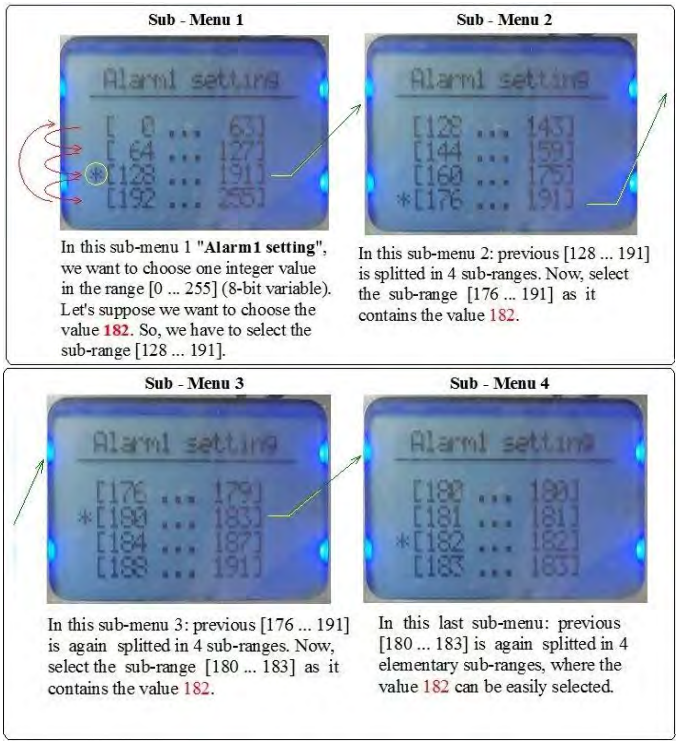

Fig.9: successive sub-range splitting allows a fast selection of an 8-bit value through 4 sub-menus with only 1 pushbutton.

To further reduce the total current consumption, we have chosen to use timer interruptions, instead of polling [27]; so, analog to digital conversions and most of the delay loops are processed in sleep mode. Last but not least, as complex computing increases power consumption, we opted to avoid it, and chose to store the 10-bit numerical count of NH_3 raw measures in RAM, which is faster and consumes less energy. Once a day (at midnight), 480 bytes are transferred to the external EEPROM. The complex calculation needed to convert these raw values into ppm NH_3 concentrations are performed on a PC after a full memory dump.

Fig.10: overview of the prototype assembly.

II.3- The conversion to ppm:

As mentioned above, the sensing resistor Rs is high in a healthy environment, but drops in the presence of the target gas, as shown in the following figure (test gas conditions: at 20±2°C, 65±5%RH).

Pt A = (10, 0.7)
Pt B = (1000, 0.09)

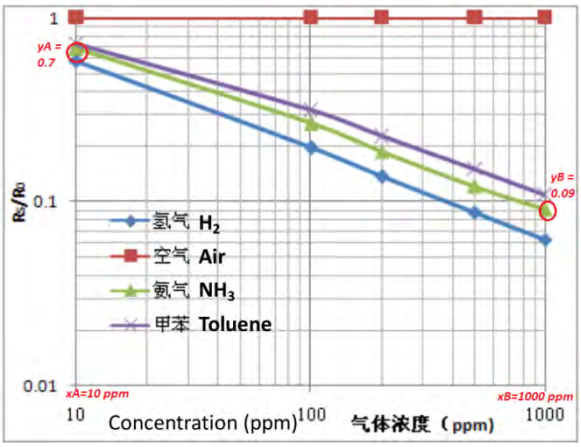

Fig.11: Sensitivity characteristic curve: gas concentration [ppm] vs ratio Rs/Ro [14]

According to the manufacturer Winsen, the sensing resistor Rs is calculated as follow:

$$Rs = (\frac{Vcc}{VRL} - 1) * RL \qquad (1)$$

where:

VRL is the voltage across the load resistor RL, measured through the analog input AN5.

Vcc = 5.0V (supply voltage)

RL = 1 to 47 [kΩ], recommended [14].

So: $$\boldsymbol{Rs = (\frac{5.0}{VRL} - 1) * RL} \qquad (2)$$

The 10-bit numerical count (CN) from the analog input AN5 can be converted to a voltage value, with the chosen reference voltage 3.3 [V] of the PICmicro:

$$VRL = 2 * \frac{(CN)}{1024} * 3300 = (CN) * 6.44 \quad \text{in [mV]} \qquad (3)$$

in a clean air, we obtained a measure of VRL = 1.1 [V],
so: Rs = 3.54 * RL [Ω].

Looking at the sensitivity characteristic curve above, the ratio Rs/Ro = 0.7 in a clean air (10 ppm),
so : Ro = Rs / 0.7 => Ro = 5.06*RL [Ω].

As the curve is given in Log/Log, let point A = (xA, yA) and point B = (xB, yB), where:

TABLE 1:
Typical points A, B coordinates and the corresponding slopes AB

	x		y	
point A	Log(10) =	1,000	Log(0.7) =	-0,155
point B	Log(1000)	3,000	Log(0.09)	-1,046

and the slope AB is

slope AB	-0,445

So, if we consider the slope AB, then:

$$slopeAB = \frac{(\text{Log}(\frac{Rs}{Ro}) - yA)}{(\text{Log}(ppm) - xA)} = \frac{(\text{Log}(\frac{Rs}{Ro}) + 0.155)}{(\text{Log}(ppm) - 1)} = -0.445 \qquad (4)$$

Finally:

$$Log(ppm) = \frac{(\text{Log}(\frac{Rs}{Ro}) + 0.155)}{-0.445} + 1$$
$$= \frac{(\text{Log}(Rs) - \text{Log}(5.06 * RL) + 0.155 - 0.445)}{-0.445}$$
$$= \frac{(\text{Log}(Rs) - \text{Log}(RL) - 0.994)}{-0.445}$$
$$= \boldsymbol{-2.247 * (\text{Log}(Rs) - \text{Log}(RL)) + 2.235}$$

So:

$$\boldsymbol{Log(ppm) = -2.247 * \text{Log}(\frac{5000}{CN * 6.4} - 1) + 2.235} \qquad (5)$$

Let's denote by *M* the calculated value of expression *(5)*, then: $$\boldsymbol{ppm = 10^{(M)}} \qquad (6)$$

Notice that Log(RL) has been canceled, and doesn't appear in the finale relation *(5)* between the measured 10-bit numerical count **CN** and the calculated value **ppm** (target gas concentration under observation). With the last expression, we notice also that the max. value of CN (1023) gives 275 ppm. Hence, our datalogger exhibits a practical useful and sufficient target range 0 … 275 ppm (keeping in mind that over 280 ppm, 1 minute exposure, irreversible health issues occur, according to AEGL-2 guideline [28]). This observation is also useful when we must optimize the datalogger storage memory (we choose 9-bit instead of 10-bit to store the ppm values).

Finally, to develop a fast and easy C code, a look-up table (LUT) of 1kB values (each pointer to this LUT is simply the CN value) is the best choice for a microcontroller, in order to obtain a fast conversion from the CN values to the corresponding meaningful values in ppm. (fast execution time means also more time allowed to the deep-sleep period, so lower power consumption).

Now, to increase the precision of these measures, temperature and humidity dependency must be considered. In our region (Oran-Arzew-Mostaganem axis), the humidity dependency may be omitted, due to the annual small variation of the relative humidity [29] (mean value per month kept between 63% and 74%, since 1999). In most of the other parts of our world, the relative humidity is lying between 46 and 80% [30], and the ratio Rs/Ro decrease is less than 10% (according to Fig.4 shown in the MQ-135 datasheet), so we may also omit the humidity dependency elsewhere.

The following empirical method consist of multiplying the Rs/Ro ratio with a coefficient **K**, extracted from Fig.4 shown in the MQ-135 datasheet, between temperatures -10°C to +50°C.

TABLE 2:
Coefficient multiplier K for Rs/Ro at different temperature

T [°C]	-10	0	10	***20***	30	40	50
Rs/Ro	1,55	1,25	1,05	***0,9***	0,85	0,83	0,8
coeff.K	1,722	1,389	1,167	***1,000***	0,944	0,922	0,889

$$\boldsymbol{Log(ppm) = -2.247 * \left(\text{Log}\left[K * \left(\frac{Rs}{RL}\right)\right]\right) + 2.235}$$
$$\boldsymbol{= -2.247 * \left(\text{Log}(K) + \text{Log}\left(\frac{Rs}{RL}\right)\right) + 2.235}$$
$$\boldsymbol{= -2.247 * \left[\text{Log}(K) + \text{Log}\left(\frac{5000}{CN * 6.4} - 1\right)\right] + 2.235}$$
$$\boldsymbol{= -2.247 * \text{Log}(K) + M} \qquad (7)$$

where:
M is the calculated value in the previous expression ***(5)***, and **K** is the coefficient calculated according to the following table 3, which is a stepwise refinement of the above table 2.

TABLE 3:
Coefficient multiplier K for Rs/Ro from -10°C to +50°C, step 1°C

Coeff. K		Temperature [°C]					
		-10	0	10	20	30	40
delta T [°C]	0	1,722	1,389	1,167	1,000	0,944	0,922
	1	1,689	1,367	1,150	0,994	0,942	0,919
	2	1,656	1,344	1,133	0,989	0,940	0,916
	3	1,622	1,322	1,117	0,983	0,938	0,912
	4	1,589	1,300	1,100	0,978	0,936	0,909
	5	1,556	1,278	1,083	0,972	0,933	0,906
	6	1,522	1,256	1,067	0,967	0,931	0,902
	7	1,489	1,233	1,050	0,961	0,929	0,899
	8	1,456	1,211	1,033	0,956	0,927	0,896
	9	1,422	1,189	1,017	0,950	0,924	0,892

In the above table 3, we extrapoled the successive values of the coefficient **K** for each decade of temperature.

then:

$$\boldsymbol{ppm = 10^{(-2.247*Log(K)+M)} = 10^{(-2.247*Log(K))} * 10^{(M)} = K^{(-2.247)} * 10^{(M)} = 10^{(M)} / K^{(2.247)}} \quad (8)$$

III. RESULTS AND DISCUSSION

Some recent studies [31] [32] have underscored the significance of ammonia dispersion from industrial plants located near urban areas. In Algeria, the city of Arzew (Lat.35°86, Lon.-0°34) is well known for its petrochemical industrial plants (operational since 1973) and their characteristic flaming torches. This region is potentially exposed to a non-negligeable sources of environmental pollution, including greenhouse gases, pollutant gases, aerosols, etc… which could negatively impact the air quality in nearby large cities such as Mostaganem and Oran.

Monitoring the evolution of NH_3 concentration is just as crucial as tracking CO_2, CO, NOx, O_3 and other critical gases, along the Oran-Arzew-Mostaganem axis, particularly due to the consistently high relative humidity (exceeding 63% since 1999). This humidity dissolves dry ammonia gas and forms ammonium hydroxide, which is worse, as this later is a highly corrosive substance that poses a significant threat to many metal-based structures.

The following set of measures has been carried out in the city of Arzew during spring 2023 (March to June). We notice that high pics of concentration (over 30ppm) are rather ephemera (less than 1 day) which make us assume that this is probably related to ammonia gas, knowing that this gas, once emitted, stays in the atmosphere for a few hours to a few days (humidity dependent) [33] [34]. The other sensitive gases (according to MQ-135 datasheet) have much longer lifetime [35]-[38], as shown in the following table:

TABLE 4:
Average gas lifetime in the air (the MQ-135 is sensitive to NH_3, toluene, CO, CO_2, H_2)

	gas	*lifetime*
1	NH_3	few hours to a few days
2	Toluene	About 50 days
3	CO	1 to 3 months
4	CO_2	More than 50 years
5	H_2	1.4 year to 2.5 years

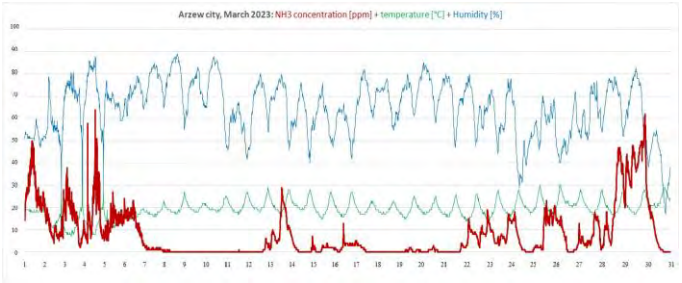

Fig.12: Ammonia concentration variation in Arzew city, March 2023.

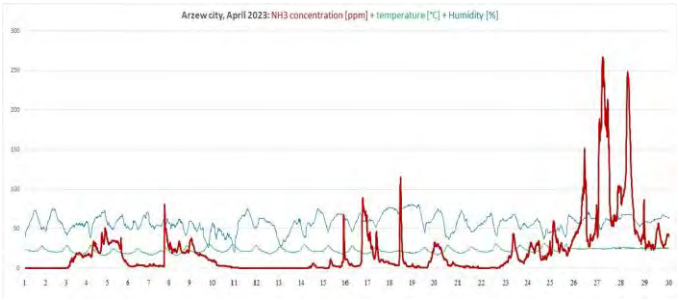

Fig.13: Ammonia concentration variation in Arzew city, April 2023.

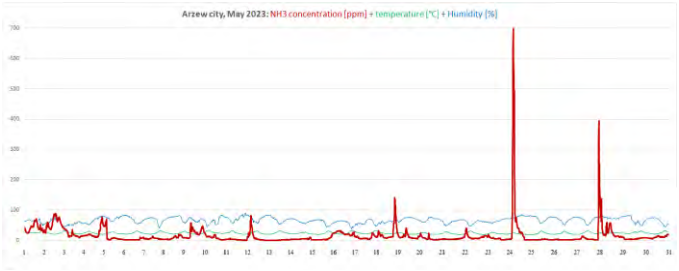

Fig.14: Ammonia concentration variation in Arzew city, May 2023.

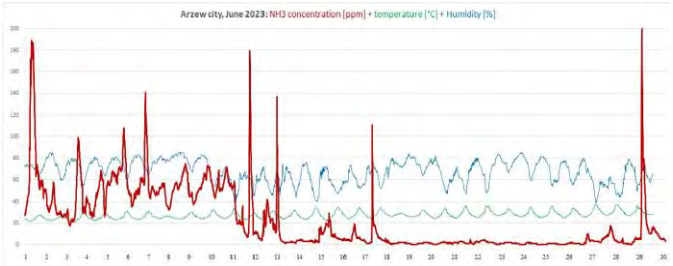

Fig.15: Ammonia concentration variation in Arzew city, June 2023.

The table below summarizes the main statistical parameters about the four months, March to June 2023. It shows that the highest mean value appeared during the month of June.

TABLE 5:
Summary of NH_3 (ppm) main statistics.

	March	April	May	June
Mean	8	21	15	22
Median	3	8	7	6
Quartile1	0	1	3	2
Quartile2	3	8	7	6
Quartile3	12	28	16	43

The following table shows a comparison between the mean ground concentrations of NH_3 collected in our study area and some other localities [39] [40]. The standard values prescribed by NIOSH (*National Institute for Occupational Safety and Health*) for NH_3 is 25 ppm over 10-hour exposure [41]. More ground level NH_3 concentration measurements in different cities obtained with different sensors are presented in [42] between 2002 and 2021.

TABLE 6:
Comparison of NH_3 mean concentrations with other localities.

Localities	NH_3 (ppm)	NH_3 (mg/m^3)	period
Arzew City	16.5	12,37	March to June 2023
Taipei City	2.41	1,807	February to Nov. 2016
Niger Delta	19.5	14,62	December 2013

Currently, global NH_3 ground level concentration monitoring networks are limited in number, and even in the most established networks, large spatial gaps exist between sites and only a few sites have records that span longer than a decade [43]. Satellites like Metop-A/B/C, Suomi-NPP, NASA-Aura, EOS Aqua, (to name a few) offer a global and bi-daily coverage data acquisition through the vertical column and at the surface, since 2002, and their on-board instruments are respectively, the IASI (Infrared Atmospheric Sounding Interferometer), the CrIS (Cross-track Infrared Sounder), the TES (Tropospheric Emission Spectrometer) and the AIRS (Atmospheric Infrared Sounder) [44]. The table shown below gives the main specifications about these satellite instruments.

TABLE 7:
main specifications about recent satellite instruments.

Satellite(instrument)	Channels	Time Coverage	Spectral range @ res. (cm^{-1})	Spatial res.(km)
Metop-A/B/C (IASI)	8461	2006 - present	645 – 2760 @ 0.5	12
Suomi-NPP (CrIS)	1305	2011 - present	645 - 2550 @ 0.625	14
NASA-Aura (TES)	43750	2004 - 2018	650 – 3050 @ 0.06	2.3
EOS Aqua (AIRS)	2378	2002 - present	650 - 2670 @ 0.5	2.3 x 13.5

The following figure shows the evolution of the atmospheric ammonia (in molec/cm^2/yr), between 2008 and 2018, from IASI data acquisition [45].

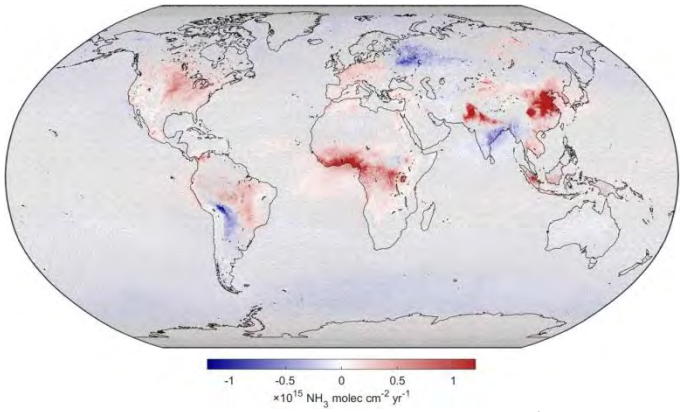

Fig.16: Evolution of the atmospheric ammonia (in molec/cm^2/yr), between 2008 and 2018.

The following table is an excerpt from the table B1 in [45] where we have retrieved data values concerning only the western Mediterranean countries, and shows that Algeria is the less concerned by NH_3 pollution during this period (while Italy exhibits the highest value, and clearly highlighted in the PO valley, figure 17).

TABLE 8:
Absolute, relative and decadal NH_3 trends measures from IASI/Metop-A.

Country	Absolute (molec/cm^2/yr)	Relative (% /yr)	Decadal (% /10yr)
Algeria	0.2 +/- 1.9 x 10^{13}	0.07 +/- 0.84	0.7 +/- 8.7
France	7.4 +/- 3.4 x 10^{13}	2.1 +/- 1.0	24 +/- 11
Italie	9.5 +/- 3.2 x 10^{13}	2.26 +/- 0.82	25.0 +/- 8.5
Morocco	1.3 +/- 2.0 x 10^{13}	0.52 +/- 0.80	5.3 +/- 8.3
Spain	7.6 +/- 2.8 x 10^{13}	2.08 +/- 0.82	22.9 +/- 8.5
Tunisia	7.6 +/- 3.8 x 10^{13}	1.74 +/- 0.90	18.8 +/- 9.4

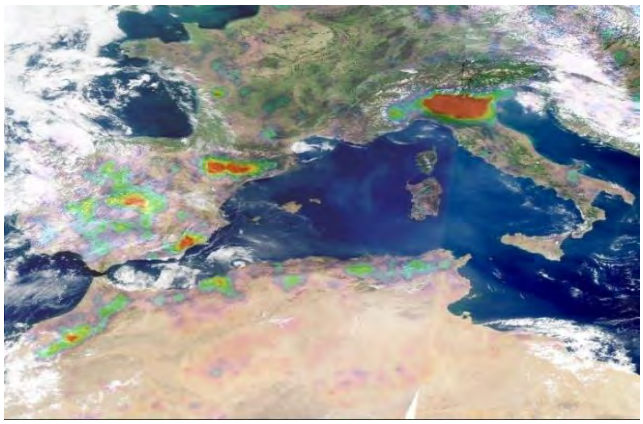
Fig.17: NH_3-IASI distributions in 2008, over the western Mediterranean countries. The yellow to red colors indicate high concentration of NH_3. [46]

Comparing measurements between ground-based points and space-based volumetric averaged pixels is a complex task that requires careful consideration of various factors [47]. Assuming a tropospheric vertical column of 10 km (in fact, varies with latitude), and knowing that the molecular weight of NH_3 is 17.031 g/mol, we can derive the following conversion from NH_3 data in molec/cm^2 to NH_3 concentrations in mg/m^3 :

$$NH_3 \text{ concentrations, in } [mg/m^3] = (M_W * T_V) / N_A \qquad \textbf{(9)}$$

Where:
M_W is the molecular weight of NH_3 = 17.031 g/mol = 17031 mg/mol.
T_V is the tropospheric vertical column, in molec/m^3, assuming equal distribution over 10^4 m altitude.
N_A is the Avogadro constant = 6.022 x 10^{23} molec/mol.

So, for NH_3 , and under 1 atmospheric pressure at 0°C temperature, we get : (case of Algeria)
Absolute [molec/m^3/yr] = 0.2 x 10^{17} ; Max. concentrations [mg/m^3] = 5.65 , equivalent to 7.54 ppm
knowing that : 1 ppm = 0.75 mg/m^3.

IV. Conclusion

In this article, we have detailed the design of a simple, low-cost and compact ammonia data logger, built around a 16-bit microcontroller, notable for its peripheral pin select feature, a low current consumption, and a range of integrated modules such as high-speed analog channels (1Mbps), PWM, 32-bit timers, etc… These features allow hardware developers to reduce the external components count, thereby keeping the prototype as compact as possible. We have also chosen a low-cost MOX type ammonia sensor rather than a more selective sensor (much higher cost) in order to lower the overall cost in the case of a mass production. This datalogger is versatile as its firmware, written in a high-level language, can be easily and slightly modified to track various other physical parameters using different types of sensors. Finally, we collected 4 months of data measures in Arzew (an Algerian petrochemical industrial city) and found that the monthly average NH_3 concentration values were below the NIOSH standard limits. This small database may be useful, as the worldwide ground-level NH_3 concentration monitoring networks are still limited, and, on the other hand, the ammonia monitoring through satellite remote sensing still has some limitations such as discontinuous temporal measurements, the presence of massive clouds affecting the measurements, the nighttime spectral measurements reduced, and some problems are related to the inference of NH_3 from the radiances detected.

References

[1]T.Liu,X. Wang, B.Wang, X.Ding, W.Deng, S.Lü, Y.Zhang, *Emission factor of ammonia (NH3) from on-road vehicles in China: tunnel tests in urban Guangzhou*. Environ. Res. Lett. 2014, *9*, 064027, doi: 10.1088/1748-9326/9/6/064027

[2] Farren N.J., Davison J., Rose R.A., Wagner R.L., Carslaw D.C. *Underestimated ammonia emissions from road vehicles.* Environ. Sci. Technol. 2020;54:15689–15697. doi: 10.1021/acs.est.0c05839

[3] Sun K., Tao L., Miller D.J., Pan D., Golston L.M., Zondlo M.A., Griffin R.J., Wallace H.W., Leong Y.J., Yang M.M., et al. *Vehicle emissions as an important urban ammonia source in the United States and China*. Environ. Sci. Technol. 2017;51:2472–2481. doi: 10.1021/acs.est.6b02805

[4] E. G. Snyder, T. H. Watkins, P. A. Solomon, E. D. Thoma, R. W. Williams, G. S. Hagler and P. W. Preuss, *The changing paradigm of air pollution monitoring, Environmental science & technology*, Vol. 47, No 20, pp. 11369-11377, 2013, doi:10.1021/es4022602

[5] P. Das, S. Ghosh, S. Chatterjee, and S. De, *A Low Cost Outdoor Air Pollution Monitoring Device with Power Controlled Built-In PM Sensor*, IEEE Sensors Journal, Vol. 22, No 13, pp. 13682 – 13695, 2022, doi: 10.1109/JSEN.2022.3175821

[6] International Energy Agency. World Balance: IEA Sankey Diagram. 2017 https://www.iea.org/Sankey/.

[7] M. Viana, J. Pey, X. Querol, A. Alastuey, F. De Leeuw, and A. Lükewille, *Natural sources of atmospheric aerosols influencing air quality across Europe*, Science of the total environment, Vol. 472, pp. 825-833, 2014, doi: 10.1016/j.scitotenv.2013.11.140.

[8] W. Knorr, F. Dentener, J. F. Lamarque, L. Jiang and A. Arneth, *Wildfire air pollution hazard during the 21st century*, Atmospheric Chemistry and Physics, Vol. 17, No 14, p. 9223-9236, 2017, doi: 10.5194/acp-17-9223-2017

[9] J. Mouly, S. Damianos & P. Delbos, *Gas and particle sensors: technology and market trends*, Market & Technology Report Ref. YINTR21178, Yole Developpement, 2021, https://s3.i-micronews.com/uploads/2021/07/YINTR21178-Gas-and-Particle-Sensors-Technology-and-Market-Trends-2021-Flyer-Yole.pdf

[10] S. Dhall, B.R. Mehta, A.K. Tyagi,K. Sood, *A review on environmental gas sensors: Materials and technologies*, Sensors International (Open access), Volume 2, 100116, 2021, doi: 10.1016/j.sintl.2021.100116

[11] Kwak, D.; Lei, Y.; Maric, R. *Ammonia gas sensors: A comprehensive review*. Talanta 2019 , 204, 713–730.

[12] Bielecki, Z.; Stacewicz, T.; Smulko, J.; Wojtas, J. *Ammonia Gas Sensors: Comparison of Solid-State and Optical Methods*. Appl. Sci. 2020, 10, 5111. https://doi.org/10.3390/app10155111

[13] *Global Ammonia (NH3) Gas Sensor Market By Type (Fixed Mount Type, Portable Type), By Application (Agriculture, Commercial), By Geographic Scope And Forecast,* Verified Market Reports website, report ID: 108448 ; 220+ pages ; Dec. 2022. https://www.verifiedmarketreports.com/product/global-ammonia-nh3-gas-sensor-market-2019-by-manufacturers-regions-type-and-application-forecast-to-2024/

[14] MQ-135 sensor datasheet, Zhengzhou Winsen Electronics Technology Co. Ltd, Version 1.4, Valid from: 2015-03-10, https://www.winsen-sensor.com/d/files/PDF/Semiconductor%20Gas%20Sensor/MQ135%20(Ver1.4)%20-%20Manual.pdf

[15] HDC1080 *Low Power, High Accuracy Digital Humidity and Temperature Sensors*, Texas Instruments, SNAS672A, 2016, https://www.ti.com/lit/ds/symlink/hdc1080.pdf?ts=1685791280117&ref_url=https%253A%252F%252Fwww.google.com%252F

[16] DS39881E datasheet: *PIC24FJ64GA004 family 28/44 pin general purpose 16-bit flash microcontrollers,* Microchip Technology Inc., May 2013, https://ww1.microchip.com/downloads/en/devicedoc/39881e.pdf

[17] XC6206 series: *Low ESR Cap. Compatible Positive Voltage Regulators*, Torex Semiconductor Ltd, ETR03005-008a, https://product.torexsemi.com/system/files/series/xc6206.pdf

[18] ME2108A *DC/DC Step-Up Converter Series*, Nanjing Micro One Electronics Inc., Datasheet Version 07, https://datasheet.lcsc.com/szlcsc/Nanjing-Micro-One-Elec-ME2108A33M3G_C236804.pdf

[19] IRF9310 datasheet: *HEXFET Power P-mosfet*, International Rectifier, PD-97437A, 2010, https://www.infineon.com/dgdl/Infineon-IRF9310-DataSheet-v01_01-EN.pdf?fileId=5546d462533600a4015356110a7d1d95

[20] DS3231 *Extremely Accurate I2C-Integrated RTC/TCXO/Crystal*, Maxim Integrated Products Inc, 2015,19-5170 Rev 10, https://www.analog.com/media/en/technical-documentation/data-sheets/DS3231.pdf

[21] 24C32 datasheet : *2-Wire Serial EEPROM 32kbit (4096x8)*, Atmel/Microchip Technology Inc., 2003, https://ww1.microchip.com/downloads/en/devicedoc/doc0336.pdf

[22] *Simple calculator for estimating a (LiPo) battery's life,* https://battery-life.of-things.de/battery-life-calculator.php

[23] *Power Profiler Kit II; Current measurement tool for embedded development, NORDIC Semiconductor ASA, Trondheim, Norway, Dec.2020,* https://www.nordicsemi.com/Products/Development-hardware/Power-

Profiler-Kit-2

[24] B. Baker, *Low-power operation is a state of mind*, EDN Electronic Design Network, AspenCore Network, 2003

https://www.edn.com/low-power-operation-is-a-state-of-mind/

[25] O. Tsekoura, G. Rebel, P. Glosek & M. Berekovic, *An evaluation of energy efficient microcontrollers*, 9th International Symposium on Reconfigurable and Communication-Centric Systems-on-Chip (ReCoSoC), Added to IEEE Xplore, ISBN:978-1-4799-5810-8, INSPEC Accession Number: 14468919, 2014, doi: 10.1109/ReCoSoC.2014.6861368

[26] H. Wu, C. Chen, K. Weng, *An Energy-Efficient Strategy for Microcontrollers*, MDPI Journals, Applied Sciences, Vol. 11, Issue 6, 2021, doi: 10.3390/app11062581

[27] B. Baker, *The power behind battery power: less than you think*, EDN Electronic Design Network, AspenCore Network, 2003. https://www.edn.com/the-power-behind-battery-power-less-than-you-think/

[28] Sylvie TISSOT, Annick PICHARD, *Seuils de toxicité aigue Ammoniac NH3*, Ministère de l'Ecologie et du Développement durable, Rapport final, INERIS, p.8/41, Aout 2003
https://substances.ineris.fr/fr/substance/getDocument/2632

[29] *ECMWF database*, Copernicus Climate Change Service Information, 1991-2021, Last refresh May 2022, https://fr.climate-data.org/afrique/algerie/oran/oran-540/

[30] *Monthly summaries of precipitation, relative humidity and soil moisture*, COPERNICUS Climate Change Service,
https://climate.copernicus.eu/monthly-summaries-precipitation-relative-humidity-and-soil-moisture

[31] Van Damme, M., Clarisse, L., Whitburn, S., Hadji-Lazaro, J., Hurtmans, D., Clerbaux, C., and Coheur, P.-F.: *Industrial and Agricultural Ammonia Point Sources Exposed*, Nature, 564, 99–103, https://doi.org/10.1038/s41586-018-0747-1, 2018

[32] Mokbis Yamina, Talem Manar Hdjer, Rahal Farid, *Evaluation de la pollution par l'ammoniac dans la region d'Arzew*, University of Sciences and Technology of Oran – Mohamed Boudiaf, Faculty of chemistry, Master, July 2022

[33] N. Evangeliou et al.: *10-year satellite-constrained fluxes of ammonia improve performance of chemistry transport models,* Atmos. Chem. Phys., 21, 4431–4451, 23 March 2021, doi.org/10.5194/acp-21-4431-2021

[34] Z. Luo et al.: *Estimating global ammonia (NH3) emissions based on IASI observations from 2008 to 2018*, Atmos. Chem. Phys., 22, 10375–10388, 12 August 2022, doi.org/10.5194/acp-22-10375-2022

[35] Bruce E. Dumdei, Robert J. O'Brien, *Toluene degradation products in simulated atmospheric conditions*, Nature 311, 248–250, 20 September 1984, doi.org/10.1038/311248a0

[36] B. Zheng et al.: *Global atmospheric carbon monoxide budget 2000–2017 inferred from multi-species atmospheric inversions*, Earth Syst. Sci. Data, 11, 1411–1436, 18 September 2019, doi.org/10.5194/essd-11-1411-2019

[37] Mason Inman, *Carbon is forever*, Nature Climate Change 1, 156–158, 20 November 2008, doi.org/10.1038/climate.2008.122

[38] Ilissa B. Ocko, Steven P. Hamburg, *Climate consequences of hydrogen emissions*, Atmospheric Chemistry and Physics, 22, 9349–9368, 20 July 2022, doi.org/10.5194/acp-22-9349-2022, 2022.

[39] Widiana, D. R., You, S. J., Yang, H. H., Tsai, J. H., & Wang, Y. F. (2017), *Source apportionment of air pollution and characteristics of volatile organic compounds in a municipal wastewater treatment plant, North Taiwan*. Aerosol and Air Quality Research, 17(11), 2878-2890, doi.org/10.4209/aaqr.2017.09.0317

[40] Rim-Rukeh, A. (2014), *An assessment of the contribution of municipal solid waste dump sites fire to atmospheric pollution*, Open Journal of Air Pollution, 3(03), 53 , doi.org/10.4236/ojap.2014.33006

[41] The National Institute for Occupational Safety and Health (NIOSH), Ammonia: exposure limits & respirator recommendations, Page last reviewed: October 30, 2019, https://www.cdc.gov/niosh/npg/npgd0028.html

[42] Mioara Petrus, Cristina Popa, and Ana-Maria Bratu (2022), *Ammonia Concentration in Ambient Air in a Peri-Urban Area Using a Laser Photoacoustic Spectroscopy Detector*, MDPI Journals, National Center for Biotechnology Information, 2022 May; 15(9): 3182, Published online 2022 Apr 28. doi: 10.3390/ma15093182

[43] Rui Wang, Da Pan, Xuehui Guo, Kang Sun, Lieven Clarisse, Martin Van Damme, Pierre-François Coheur, Cathy Clerbaux, Melissa Puchalski, and Mark A. Zondlo, *Bridging the spatial gaps of the Ammonia Monitoring Network using satellite ammonia measurements*, EGUsphere, https://doi.org/10.5194/egusphere-2023-190, 2023

[44] Warner, J. X., Wei, Z., Larrabee Strow, L., Dickerson, R. R., and Nowak, J. B., *The global tropospheric ammonia distribution as seen in the 13-year AIRS measurement record*, Atmos. Chem. Phys., 16, 5467–5479, https://doi.org/10.5194/acp16-5467-2016, 2016

[45] Martin Van Damme et al, *Global, regional and national trends of atmospheric ammonia derived from a decadal (2008–2018) satellite record*, Environmental Research Letters, May 06th, 2021, Vol.16, N°5, 055017, https://doi.org/10.1088/1748-9326/abd5e0

[46] The European Space Agency, *Satellite sensor maps global atmospheric ammonia emissions*, 07/07/2009,
https://www.esa.int/Applications/Observing_the_Earth/Satellite_sensor_maps_global_atmospheric_ammonia_emissions

[47] Schiferl, L. D., Heald, C. L., Damme, M. van, Clarisse, L., Clerbaux, C., Coheur, P., Nowak, J. B., Neuman, J. A., Herndon, S. C., Roscioli, J. R., and Eilerman, S. J, *Interannual variability of ammonia concentrations over the United States : sources and implications*, Atmos. Chem. Phys., 12305–12328, https://doi.org/10.5194/acp-16-12305-2016, 2016

Noureddine BENABADJI
My first job was a teacher at the Intitute of Telecommunications - Oran (I.T.O) from 1984 to 1999, where I taught the following courses: Electricity, Tests & Measurements, Electronic components, Electronic circuits, Logic circuits, Computer Hardware, Microprocessors, Assembleur programming (8086), Algorithms and programming in C.

My second job now is a teacher/researcher at the University of Sciences & Technology - Oran (U.S.T.O) where I teach C.A.D (using AutoCAD software) and doing R & D in the laboratory LAAR (Laboratory of Analysis & Applications of Radiations) where my research team has designed a local station in order to receive multispectral images from polar and geostationnay satellites like NOAA and METEOSAT, and developped several image processing softwares (PCSATWIN, PCNOAA, MSGVIEW, COMPACTA, ...). In the other hand, several electronic prototypes have been designed to support this local station.
https://orcid.org/0000-0001-7337-6410
https://scholar.google.com/citations?user=py_M3zEAAAAJ&hl=fr&oi=ao

Farid RAHAL
Dr. Farid RAHAL is Lecturer at the Department of Architecture of the University of Sciences and Technologies at Oran Mohamed BOUDIAF in Algeria. He teaches students in architecture, modeling and geomatics. The main focus of his research concerns air quality. He has worked on emission inventories, meteorological modeling, pollutant transport modeling and air quality monitoring by micro- sensors. He also worked on urban sprawl using satellite images. He has developed applications in parametric design concerning architecture. Finally, he worked on urban and environmental risks.
https://orcid.org/ 0000-0001-7495-8324
https://scholar.google.com/citations?user=csWoIBUAAAAJ&h l=fr
https://www.researchgate.net/profile/Farid_Rahal
farid.rahal@univ-usto.dz

Imane Nadjah MENAKH
PhD student in the laboratory LAAR (Laboratory of Analysis & Applications of Radiations) at the University of Sciences and Technologies of Oran-Mohamed BOUDIAF- (Algeria). Her research areas focuses on the field of physics, technology, and radiation. She holds a Master's degree, with a thesis presented in June 2018 titled "Analysis of transport phenomena in the GaSb/ GaAlAsSb system, used in radiation detectors around 1.7 µm ".
naineblanche28@.outlook.fr
imanenadjah.menakh@univ-usto.dz